

Deliverable D 3.8

Comparison between the methods for masonry computations

Document type	Deliverable D 3.8
Document Version / Status	1.8
Primary Authors	João Pereira, jpereira@civil.uminho.pt, UMINHO
Distribution Level	PU (Public)
Project Acronym	ATHOR
Project Title	Advanced THERmomechanical multiscale mOdelling of Refractory linings
Grant Agreement Number	764987
Project Website	www.etn-athor.eu
Project Coordinator	Marc Huger, marc.huger@unilim.fr, UNILIM
Document Contributors	João Pereira, jpereira@civil.uminho.pt, UMINHO
	Pratik Gajjar, pratik.gajjar@civil.uminho.pt, UMINHO
	Mahmoud Ali, mahmoud.ali@univ-orleans.fr, UORL
	Alain Gasser, alain.gasser@univ-orleans.fr, UORL

History of Changes

Version	Date	Author (Organization)	Change	Page
1.0	09.03.2022	Pratik GAJJAR (UMinho) Mahmoud Ali (UORL)	First draft	All
1.1	14.03.2022	João Pereira (UMinho)	Review	All
1.2	15.03.2022	Pratik GAJJAR (UMinho)	Revision	All
1.3	16.03.2022	Alain Gasser (UORL)	Review	All
1.4	16.03.2022	Pratik GAJJAR (UMinho)	Revision	All
1.5	24.03.2022	Mahmoud ALI (UORL)	Revision	All
1.6	24.03.2022	Pratik GAJJAR (UMinho)	Revision	All
1.7	25.03.2022	Glyn DERRICK (UNILIM)	Formatting and English check	All
1.8	28.03.2022	Glyn DERRICK (UNILIM) Marc HUGER (UNILIM)	Final check	All

TABLE OF CONTENTS

1 INTRODUCTION.....	2
2 SHORT SUMMARY OF THE METHODOLOGY.....	2
2.1 Materials	2
2.2 Modelling approaches	3
3 WALLETS UNDER VERTICAL UNIAXIAL SETUP	5
3.1 Brief description of the experimental setup	5
3.2 S01.AT.LBC: uniaxial compression up to failure at room temperature	5
3.3 S03.HT.LL8: uniaxial compression at high temperature	6
4 WALLETS IN HORIZONTAL BIAXIAL SETUP.....	7
4.1 Brief description of the experimental setup	7
4.2 S06.AT.LBJ: uniaxial loading and unloading - normal to bed joints at room temperature	9
4.3 S07.AT.LHJ: uniaxial loading and unloading - normal to head joints at room temperature	10
4.4 S08.AT.LBI: biaxial loading and unloading at room temperature.....	11
4.5 S09.HT.CBJ: uniaxial creep behaviour - normal to bed joints	12
4.6 S10.HT.CBI: biaxial creep behaviour.....	14
4.7 S11.HT.RBI: biaxial relaxation behaviour	16
4.8 Comparisons of the computational time	16
5 CONCLUSIONS.....	17
6 REFERENCES.....	17

1 Introduction

This report presents a comparison between different modelling approaches used to simulate the thermomechanical behaviour of refractory masonry under extreme conditions. The subjects used for the comparison are the uniaxial masonry panels tested at UMINHO and the bi-axial panels tested at RHI-Magnesita. These experimental campaigns have been described previously in [Deliverable D4.3](#) - Thermomechanical characterization of subsystems finished.

Different modelling approaches, considering micro and macro modelling, were used, and are compared in this document. These include homogenization at the macro level and different FEM software at the micro level. These modelling approaches have already been described in [Deliverable D3.6](#) - Model of the non-linear behaviour of masonry at high temperature.

This document gathers a summary of the description of the modelling approaches as well as a summary of the experimental setups. For detailed information regarding the modelling approaches and/or the experimental setups, refer to the previously mentioned documents.

2 Short summary of the methodology

This section presents a brief description of the material properties considered in the experimental and numerical studies, as well as a summary of the modelling approaches used for this comparison.

2.1 Materials

Refractory masonry walls built with alumina spinel cuboid bricks are studied in the present work. The bricks were produced by RHI-Magnesita. They have been fully characterized within the ATHOR network. The chemical composition of the material is 94 wt % alumina, 5 wt % magnesia and 1 wt % other oxide such as iron oxide and silica. The apparent porosity and density of the material are 19 % and 3.13 g/cm³, respectively [1]. The thermal conductivity and specific heat of the material properties are shown in Figure 1-a and b [2]. The Young's modulus measured using the ultra-sound technique [3] and mechanical tests, and the ultimate compressive stress [4] variations with temperature are presented in Figure 1- c and d, respectively. The values of Young's modulus measured using mechanical tests are preferred and will be used later in the present work while developing the numerical

models. Other properties, such as, friction coefficients (dry joints) and creep parameters are mentioned in detail in *Deliverable D3.6*.

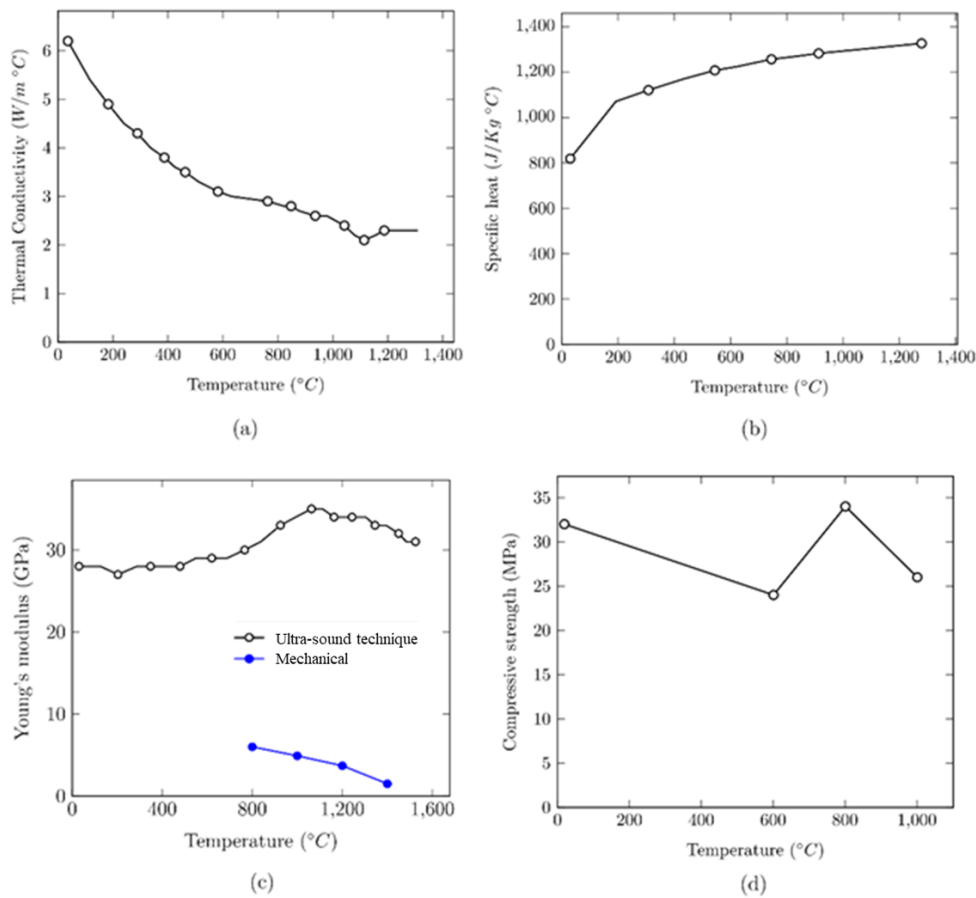


Figure 1 - Thermal and mechanical properties of alumina spinel bricks tested in the present work: (a) thermal conductivity [2] (b) specific heat [2], (c) Young's modulus [3] and (d) ultimate compressive strength [4].

2.2 Modelling approaches

Masonry structures are composed of units and joints. They feature a wide variety of combinations with different component materials, geometry, and textures. These combinations imply a significant number of descriptive material parameters, thus, presenting itself as a complex research field [5]. Therefore, the importance of sophisticated numerical tools capable of predicting the behaviour of the masonry from the linear stage, through cracking and degradation until complete loss of strength [6]. However, in the 1990s, the masonry research community began to show interest in sophisticated numerical tools to study masonry instead of the prevailing tradition of rules-of-thumb and empirical formulae [6].

As a composite material, masonry has certain particularities that make it challenging to adapt existing numerical tools from more advanced research fields, such as the mechanics of concrete, rock, and composite materials. Therefore, the necessity for different approaches. Due to the heterogeneous states of stress and strain in a masonry structure, it is crucial to assess the local behaviour of the masonry with mortar through a detailed micro-model. Mechanical properties of both the unit and mortar and the interface between them could be considered in this model (Figure 2a). This approach, however, is only adequate for small structural elements. Alternatively, a simplified micro-modelling approach (Figure 2b) can be adopted to address the disadvantages of the detailed micro approach. In the simplified procedure, the units are expanded by adding the mortar thickness. The expanded units are modelled as a series of continuum elements. The interaction between the expanded units is modelled as a series of interface elements. In the case of large structures (such as steel ladle), the knowledge of the interaction between units and mortar is negligible for global structural behaviour. Therefore, a different approach, denoted macro-modelling, can be used. In this approach, the material is regarded as an anisotropic composite, and a relation is established between average masonry strains and average masonry stresses (Figure 2c). This is a phenomenological approach, meaning that the material parameters must be obtained from masonry tests of sufficiently large size under homogeneous states of stress. A complete macro-model must

reproduce an orthotropic material with different tensile and compressive strengths along the material axes and different inelastic behaviour for each material axis [6].

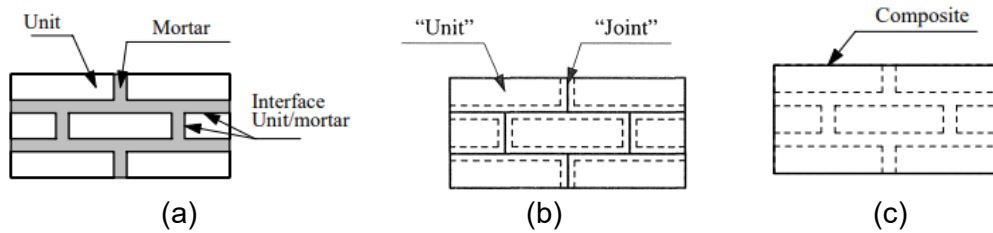


Figure 2 - Modelling strategies for masonry structures [6]:
(a) detailed micro-modelling; (b) simplified micro-modelling; (c) macro-modelling.

2.2.1 Micro-modelling approach used at UMINHO

As the tests were performed with a mortarless refractory masonry wall, a simplified micro-modelling approach (Figure 2b) is adopted here. In this approach, the spatial discretization of the masonry is performed at the level of brick elements, and the dry joints are represented by their contact behaviour using interface elements. Herein, brick elements are simulated with corresponding mechanical parameters of the material from which they are made and their connection with contact elements that permit separation, penetration, and sliding at the contact.

In this micro-modelling approach, the units are modelled as continuum elements. The interfaces between bricks are represented by discontinuous elements. Even though accurate results are obtained using the micro-modelling technique, the main drawback is the extensive computational resources required to run the analysis [7], [8]. Nevertheless, this approach provides detailed results on the behaviour of the bricks and joints and with the advances in computational resources this has become possible even for larger structures. The numerical analyses for this approach are performed using two different finite element software, Abaqus [9] and DIANA FEA [10]. These software contain an extensive multi-purpose finite element software package that can be utilised in a wide range of engineering sectors. *Deliverable D3.6* lists further modelling considerations for this micro-modelling approach.

2.2.2 Homogenization approach at UORL

Refractory masonry with dry joints has strongly nonlinear stress-strain relationships due to gradual closure of joints and markedly orthotropic behaviour (caused by the difference between the number of bed and head joints and the fact that they can be closed in one direction and open in the other direction). To numerically capture such nonlinear phenomena and consider the impacts of gradual joint closure/reopening on the homogenized mechanical response, four periodic joint patterns, as well as transition criteria between them, were defined as depicted in Figure 3. Each pattern is associated with a specific state of bed and head joints (open or closed) and represents different periodic masonry structure with different equivalent elastic viscoplastic behaviour. The predefined patterns are:

1. Pattern AC: All joints are Closed.
2. Pattern BO: Bed joints are Open.
3. Pattern HO: Head joints are Open.
4. Pattern AO: All joints are Open.

Further detail of nonlinear homogenization approach and joint opening and closing criterion can be found in *Deliverable D3.6*.

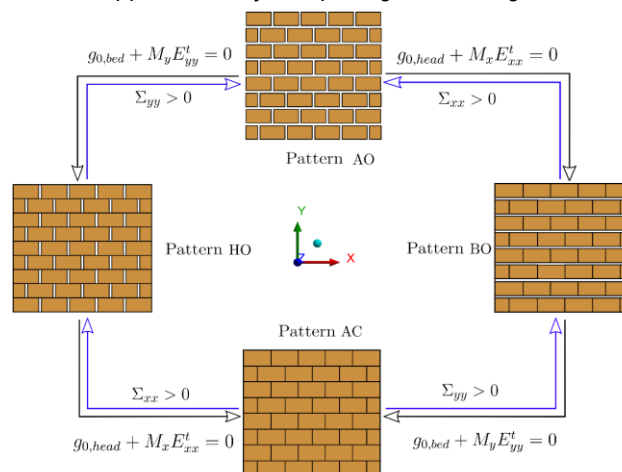


Figure 3 - Schematics of all possible joint patterns of refractory masonry with dry joints and joints closure and reopening criteria.

3 Wallets under vertical uniaxial setup

This section presents a brief description of the experimental setup and the obtained results from the comparison of the different modelling approaches. Here, for the uniaxial tests, DIANA FEA [10] was used for the micro-modelling approach.

3.1 Brief description of the experimental setup

The experimental tests were carried out at the Laboratory of Testing Materials of the University of Coimbra, in Portugal. A general overview of the test setup can be seen in Figure 4. The test set-up consists of one reaction frame composed by two HEB500 columns and two overlapping HEB600 beams (4500 mm span). The hydraulic jack had the capacity of 3 MN and the load cell used to measure the applied load had the capacity of 5 MN. For the experiments performed at high temperatures one modular electric furnace (45 kVA) was used to heat the specimens. Additional details regarding the experimental setup, the specimens and the acquisition systems can be seen in *Deliverable D4.3*. When referring to the numerical results, the name for every test series was kept the same for ease of understanding and following both this deliverable and *Deliverable D4.3*.

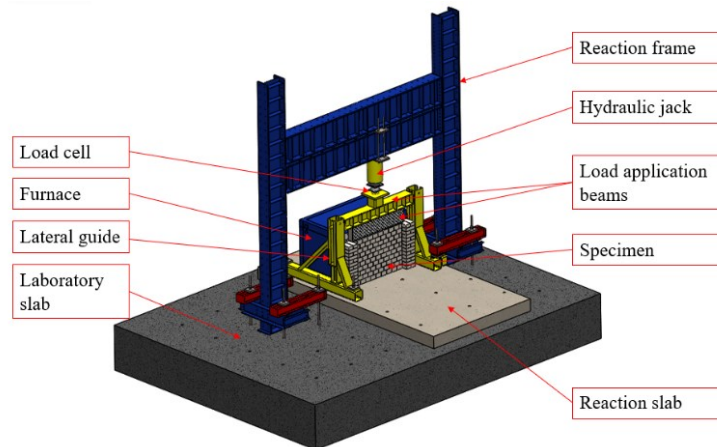


Figure 4 - Experimental setup used to perform uniaxial compression tests of alumina spinel refractory masonry walls.

From the experimental programme developed in the scope of ATHOR, which intended to assess the loadbearing capacity of the walls at high temperatures in service conditions, two uniaxial tests were chosen to be simulated here. The first one is series S01.AT.LBC, a uniaxial compressive test carried at room temperature, which aimed to assess the loadbearing capacity of the wall. The other test selected here is series S03.HT.LL8, being carried out at high temperatures and aimed to assess the thermomechanical behaviour of the masonry under a constant load level. Firstly, a mechanical load of 8 MPa was applied to the specimen, then the wall was heated up according to ISO 834-1 [11]. The walls geometry is presented in Figure 5.

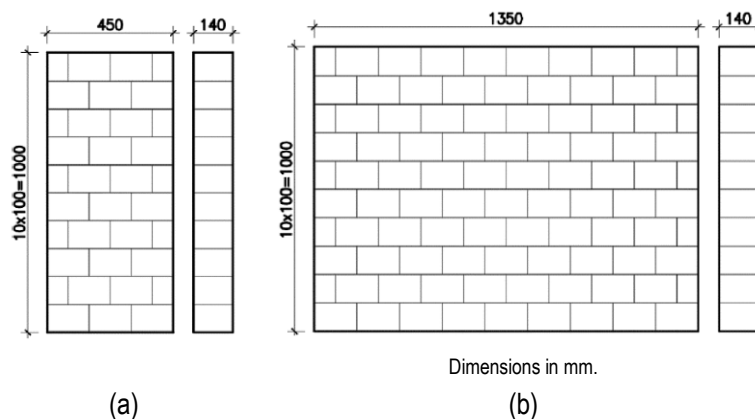


Figure 5 - Specimen's dimensions, (a) Series S01.AT.LBC; (b) Series S03.HT.LL8 [12].

3.2 S01.AT.LBC: uniaxial compression up to failure at room temperature

In this test series, three refractory masonry walls with dimensions $450 \times 1000 \times 140 \text{ mm}^3$ (Figure 5a) were tested up to failure. The objective of this test series was to assess the loadbearing capacity of the refractory masonry walls. The test procedure in series S01.AT.LBC had the following steps: i) the masonry specimens were built in the testing system; ii) the loading beams were placed

on the top of the specimens using a crane; iii) the instrumentation was installed; iv) the loadbearing capacity test was performed under displacement control at a rate of 0.01 mm/s up to failure of the specimen.

A detailed description of the FE models for both the micro and macro approach is given in *Deliverable D3.6*. Here, the focus is on the results and comparison between modelling approaches.

The vertical displacement fields predicted by the numerical models (in the direction normal to bed joints - loading direction) on the front surface of the wall, at maximum load level, are presented in Figure 6. It can be noticed from the micro-model that for this force level, bricks primarily behave as a rigid body and most of the displacement observed is due to closing of the dry joints. Comparisons between the experimental and numerical force-displacement curves are shown in Figure 7. The displacements of the experimental tests were determined from the LVDT. Good agreements between the experimental and numerical results can be observed. It can be noticed that both numerical models can reproduce, with reasonable accuracy, the nonlinear mechanical response of the wall. The resulting force displacement diagram of the wall is nonlinear; the stiffening behaviour of the wall is caused by the progressive closure of joints and the gradual increase in the contact area with the increase of the applied load (increase of effective stiffness). It seems clear that both approaches are able to represent the experimental behaviour and are quite similar to one another.

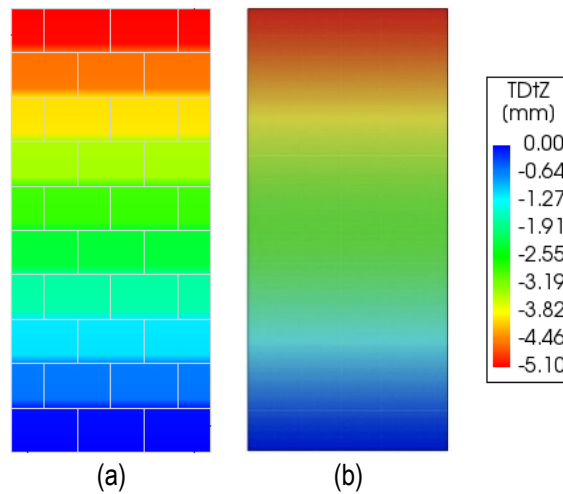


Figure 6 - Test series S01.AT.LBC, vertical displacement fields in masonry wall subjected to uniaxial compression load in the vertical direction maximum load level: a) Micro-model; b) Macro-model.

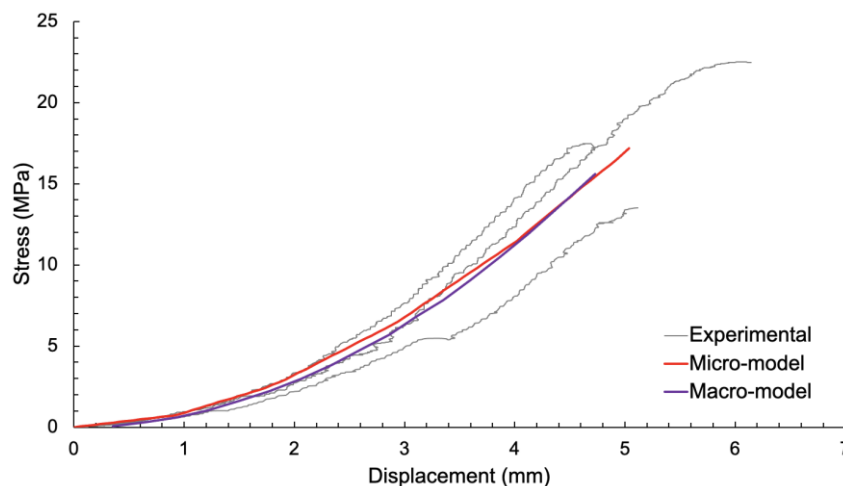


Figure 7 - Test series S01.AT.LBC, displacement, in the direction normal to bed joints, versus vertical reaction force in an alumina spinel masonry wall subjected to uniaxial compression load, up to failure, at room temperature, experimental and numerical results.

3.3 S03.HT.LL8: uniaxial compression at high temperature

In this test series, three refractory masonry walls with dimensions 1350×1000×140 mm³ (Figure 5b) were tested. Series S03.HT.LL8 was tested at high temperatures. Steps i, ii and iii of the test procedures were similar to those presented for series

S01.AT.LBC. Then: iv) the specimen was loaded under displacement control at a rate of 0.01 mm/s up to 8 MPa at ambient temperature, v) the control procedure was changed to load control and set to keep the current load; vi) the furnace was turned on and the specimen was heated according to the standard fire curve ISO 834-1 [11]; vii) the wall was monitored for five hours: the temperatures, applied load and in-plane displacements were recorded. The specimens were not tested up to the failure due to limitations on the maximum operating time of the furnace.

A detailed description of the FE models for both the micro and macro approach is given in *Deliverable D3.6*. Here, the focus is on the results and comparison between modelling approaches.

The comparison of the in-plane displacements, on top of the masonry wall, obtained experimentally and numerically are presented in Figure 8. At the beginning of the test, from 0 to 1200 s, as the pre-compression stress of 8 MPa was applied, negative displacements were observed because of the joint closure and bricks' deformation. The furnace was then turned on and the temperatures at the hot face started to increase. With the beginning of the heating procedure, the effects of the thermal elongation started to increase, and the wall presented a positive strain rate. During the period between 1200 s to 2700 s, there are some differences among the numerical and experimental in-plane displacements, that may have been caused by rotation of the load application beam in its longitudinal axis, induced by the beginning of the thermal bowing of the wall. Nevertheless, both the developed models can represent all stages of the test, including the effects of the thermal elongation on the masonry walls. At around 16000 seconds, the thermal expansion effects of the wall over passed the impact of mechanical load application and a positive displacement was recorded by the LVDTs and predicted by the present models. Micro-model predicts a vertical displacement of 4 mm compared to 3.5 mm of macro-model; this difference is mainly due to the different joint closure criterion employed by these models. Moreover, during thermal load application, macro-model predicts a linear expansion of the wall compared to a non-linear response from micro-model, this difference is due to the applied boundary conditions and nonlinear homogenisation strategy employed for macro-model.

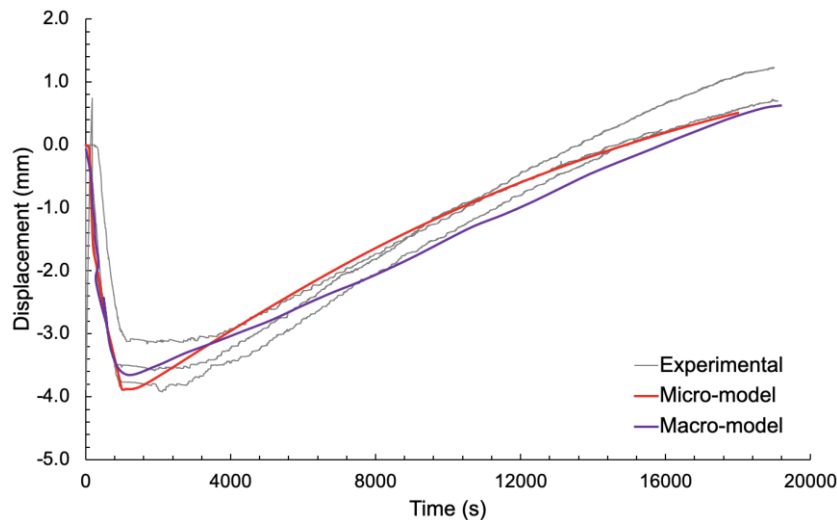


Figure 8 - Test series S03.HT.LL8, experimental and numerical time variations of the vertical displacement.

4 Wallets in horizontal biaxial setup

This section presents a brief description of the experimental setup and the obtained results from the comparison of the different modelling approaches. Here, for the bi-axial tests, Abaqus [9] was used for the micro-modelling approach.

4.1 Brief description of the experimental setup

These experimental tests were carried out at the Technology Centre Leoben (TCL) of RHI-Magnesita, in Austria. The schematic overview of the test setup is presented in Figure 9. The test setup consisted of a monolithic reaction frame in which the hydraulic jacks, LVDTs and heating system were connected. Two orthogonal hydraulic jacks with the capacity of 1000 kN were used, with a Rexroth controller unit. The applied forces were measured by two pressure gauges per cylinder. A 48-channel data acquisition system was used to record the data from the experiments. Additional details regarding the experimental setup, the specimens and the acquisition systems can be seen in *Deliverable D4.3*. When referring to the numerical results, the same name for every test series was kept the same for consistency and ease of understanding between this deliverable and *Deliverable D4.3*.

Thirteen tests of alumina spinel refractory masonry walls were performed. Six of them were performed at room temperature and the remaining eight tests were carried out at high temperature. The test series names, loading conditions in directions

perpendicular to the surfaces of bed and head joints and testing temperature are given in Table 1. For all tests, the dimensions of the walls are 1125×1100×140 mm³.

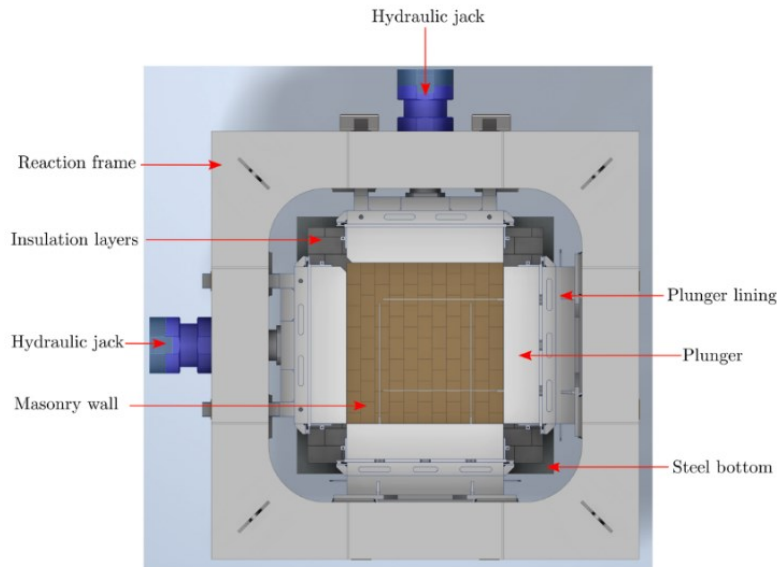


Figure 9 - Top view of the biaxial compression test field.

Table 1: Summary of the biaxial compression tests of refractory masonry walls performed at room and high temperatures.

Series	Specimen	Maximum load		Temperature
		Bed	Head	
S06.AT. LBJ	S06.AT. LBJ.01	6 MPa	Constrained	Room temperature
	S06.AT. LBJ.02			
S07.AT. LHJ	S07.AT. LHJ.01	Constrained	6 MPa	
	S07.AT. LHJ.02			
S08.AT. LBI	S08.AT. LBI.01	6 MPa	6 MPa	
	S08.AT. LBI.02			
S09.HT. CBJ	S09.HT. CBJ.01	4 MPa	Constrained	High temperature
	S09.HT. CBJ.02			
S10.HT. CBI	S10.HT. CBI.01	4 MPa	4 MPa	
	S10.HT. CBI.02			
S11.HT. RBI	S11.HT. RBI.01	4 - 6 MPa	4 - 6 MPa	
	S11.HT. RBI.02			

Using Abaqus finite element software, a series of numerical models of masonry walls subjected to cyclic in-plane uniaxial and biaxial compression loads at room temperature were developed. The purpose of these models was to reproduce the observed experimental behaviour and validate the numerical models. For the numerical simulations at ambient temperature only the elastic properties of the bricks were used. For the simulations at high temperatures, elastic-viscoplastic properties of the bricks were used. The experimental tests were modelled with the two different approaches: the micro modelling and the macro modelling approaches.

The micro and macro-FE models of the walls are shown in Figure 10. The x-direction (1125 mm) is the direction normal to head joints, while the y-direction (1100 mm) is normal to bed joints. The four ceramic plates and the insulation layer (ground) of the test setup have been modelled as rigid plates. The units (refractory bricks) and dry joints were modelled separately in the micro-model approach (Figure 10a). In the macro model, the wall (bricks and joints) was replaced by a homogeneous material (Figure 10b) whose mechanical properties depend on the state of bed and head joints (open or closed). In both models, the walls were meshed with 3D hexahedron elements (C3D8T) with 35×35×35 mm³ size element. Frictional interactions between the contact surfaces of the wall and the fixed, moving rigid plates and the ground were considered with a coefficient of friction of 0.5.

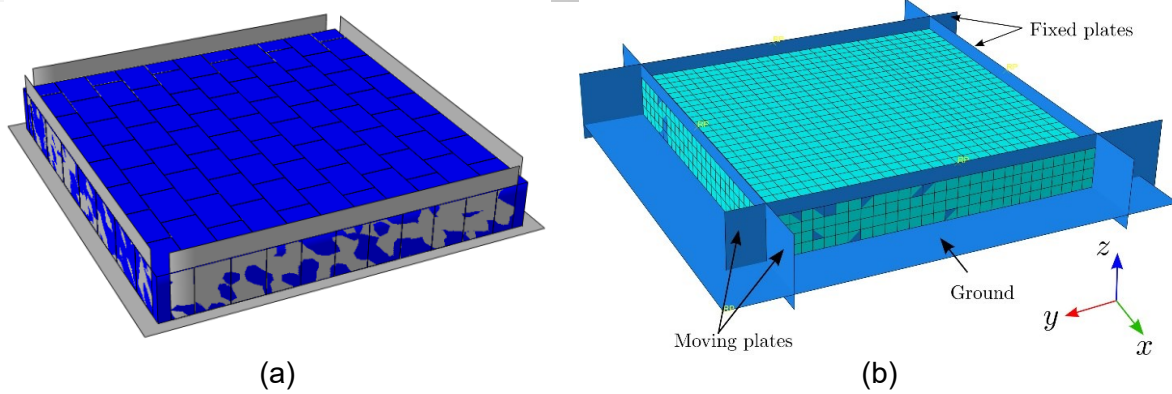


Figure 10 - FE models of the mortarless refractory masonry walls: a) Micro-model; b) Macro-model.

4.2 S06.AT.LBJ: uniaxial loading and unloading - normal to bed joints at room temperature

In this test series, two refractory masonry walls were tested. A cyclic (load/unload) uniaxial compression (up to 6 MPa) was applied in the direction normal to bed joints, and the plungers constrained the direction normal to head joints. The boundary conditions for two fixed rigid plates, the rigid moving plate normal to head joints (x-direction in Figure 11a) and the ground are set to fully fixed.

Comparisons between the experimental and numerical force-displacement diagrams of masonry walls subjected to uniaxial compression loading/unloading in the direction normal to bed joints are presented in Figure 11b. The displacement values were obtained from the relative displacements of the red points shown in Figure 11a (as in the experiments). It can be seen that the present numerical models reproduce, with reasonable accuracy, the displacement stiffening mechanical behaviour of the wall. The reaction force increases with the increase in the applied displacement due to the gradual closure of the joints and the increase in effective stiffness and contact area with the closure of joints. After unloading, the wall did not recover its initial configuration and there was permanent deformation caused by the closure of joints, the deformation and the crushing of the asperities present at the contact surfaces of bed joints. Between the micro and macro modelling approaches, it can be observed that the results are similar, with the difference increasing in the unloading phase after the first cycle. However, both approaches are well within the experimental results. In the case of the macro model, only the first cycle was simulated. Further developments of the UMAT are required to consider the change of the stiffness for the second and third cycles. These developments are planned for future work.

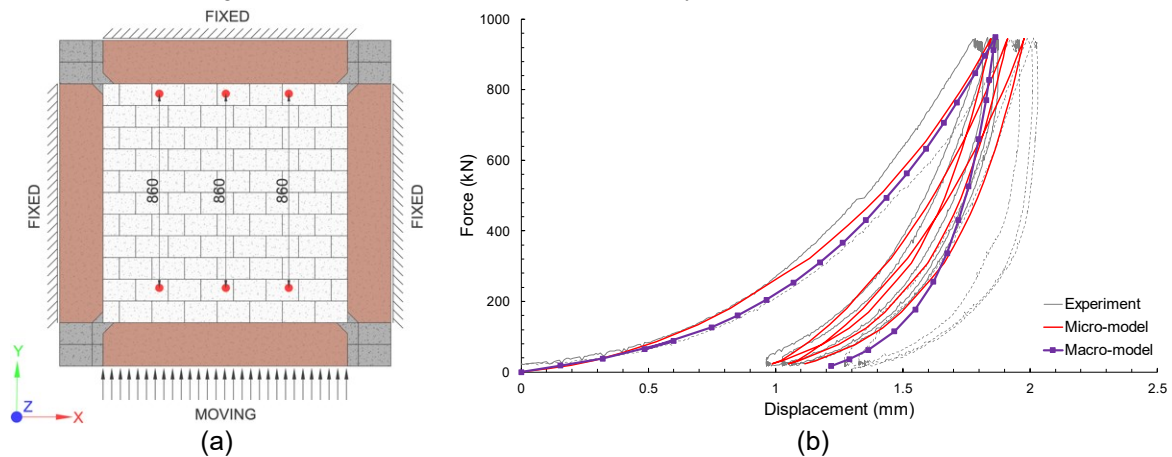


Figure 11 - Test series S06.AT. LBJ - uniaxial loading and unloading - normal to bed joints: a) Boundary conditions; b) Experimental and numerical force-displacement diagrams.

Figure 12a and b present the numerical displacement fields obtained from the micro and macro models at the maximum load level (630 kN). It can be observed from the results of the micro model that almost all the displacement occurs due to the closing of dry joints and bricks behave as a rigid units for this low level of applied stress. Figure 12c-d shows the distribution of the principal compressive (minimum) stresses at the first peak load. From the figure, it is possible to observe that the stress is distributed uniformly at around 6 MPa in the bricks except at areas near corners. This behaviour is due to the presence of chamfered ceramic plates used for support and loading. It can be observed that for both the approaches, the distribution of displacement and stress is identical.

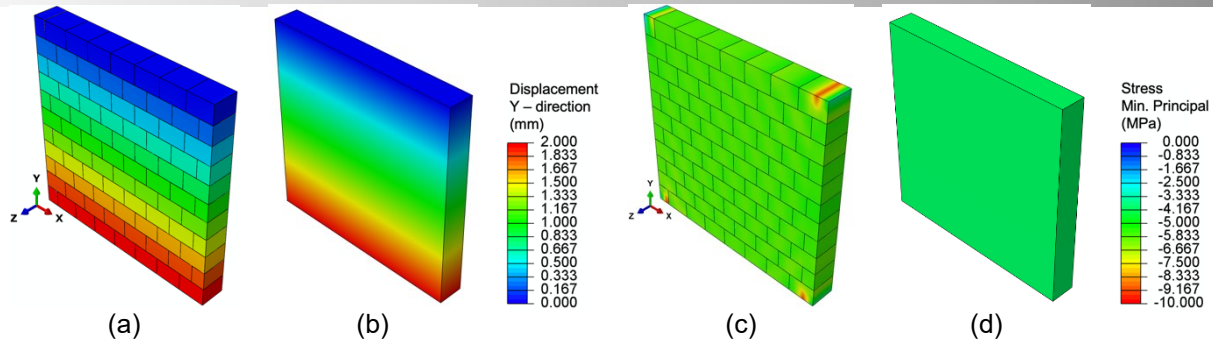


Figure 12 - Test series S06.AT.LBJ - uniaxial loading and unloading - normal to bed joints: Displacement distribution along the Y direction (mm) at the peak force: a) Micro-model; b) Macro-model. Minimum principal stress distribution (MPa) at the peak force: c) Micro-model; d) Macro-model

4.3 S07.AT.LHJ: uniaxial loading and unloading - normal to head joints at room temperature

Regarding this test series, two refractory masonry walls were tested at room temperature. The main difference between S07.AT.LHJ and S06.AT.LBJ is that the uniaxial compression loading (6 MPa) and unloading were applied to the direction normal to head joints while the other direction (normal to bed joints) was constrained by the ceramic plungers. The boundary conditions of two fixed rigid plates, the moving rigid plate normal to bed joints (y-direction in Figure 13a) and the ground, are fully fixed.

Comparisons between the experimental and the numerical force-displacement diagrams of the walls subjected to uniaxial compression loading/unloading in the direction normal to head joints are given in Figure 13b. The numerical models were able to predict the mechanical behaviour of the walls (for both the loading and unloading) with reasonable accuracy. As compared to S06.AT.LBJ, the value of the displacement at the maximum load level is lower. This can be attributed to the number of head joints in the wall being less than the number of bed joints (7 head joints and 10 bed joints). This leads to higher stiffness (and, therefore, less deformation at the same load level) in the direction normal to head joints as compared to the direction normal to bed joints. After unloading and as observed in S06.AT.LBJ, the walls did not go back to the initial configuration and there was permanent deformation. In this series, although both models are within the experimental results, the macro-model predicts a stiffer response compared to the micro-model, the difference can be due to the joint closure relations.

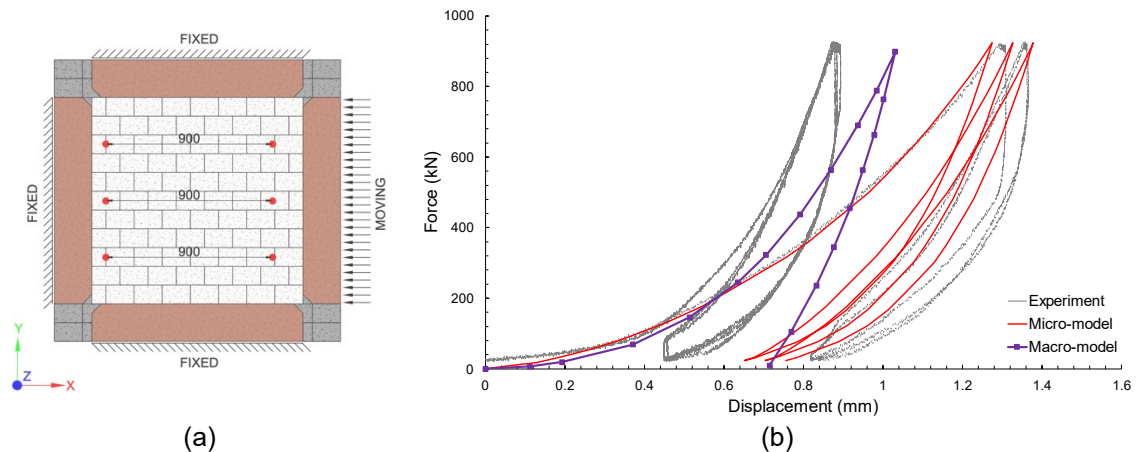


Figure 13 - Test series S07.AT.LHJ - uniaxial loading and unloading - normal to head joints: a) Boundary conditions; b) Experimental and numerical force-displacement diagrams.

Figure 14a and b show the displacement fields, obtained using both modelling approaches, in the walls at maximum load level. In the micro model, the bricks behave almost as rigid units for a low level of stress. Figure 14c and d show the distribution of the principal compressive stresses at the first peak load. From the figure, it is possible to observe that the stress is distributed uniformly at 6 MPa in the bricks except at areas near the support plates. This high concentration can be explained due to the presence of chamfered ceramic plates used for support and loading. Moreover, both models describe similar distribution of stress and displacement in the masonry wall.

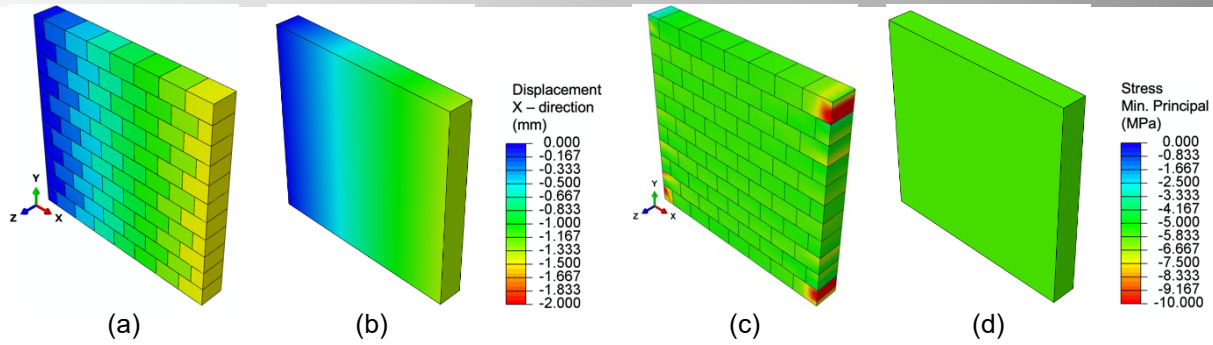


Figure 14 - Test series S07.AT.LHJ – uniaxial loading and unloading – normal to head joints:
Displacement distribution along the Y direction (mm) at the peak force: a) Micro-model; b) Macro-model.
Minimum principal stress distribution (MPa) at the peak force: c) Micro-model; d) Macro-model

4.4 S08.AT.LBI: biaxial loading and unloading at room temperature

In this test series, two refractory masonry walls were tested at room temperature. A 6 MPa biaxial compression load/unload was applied to the directions normal to bed and head joints. The boundary conditions of the ground and the two fixed rigid plates are fully fixed (Figure 15a).

Figure 15b presents a comparison between the experimental and numerical force-displacement diagrams in the directions normal to bed and head joints during loading and unloading. The present numerical models can reproduce with reasonable accuracy the orthotropic displacement stiffening mechanical behaviour of the wall. The reaction force increases with an increase in displacement due to the gradual closure of the joints and an increase in material stiffness with the gradual closure of joints. The maximum displacement in the direction normal to head joints is smaller than that in the direction normal to bed joints due to the number of joints. Similar to S06.AT.LBJ and S07.AT.LHJ, there were permanent deformations in the directions normal to bed and head joints after unloading.

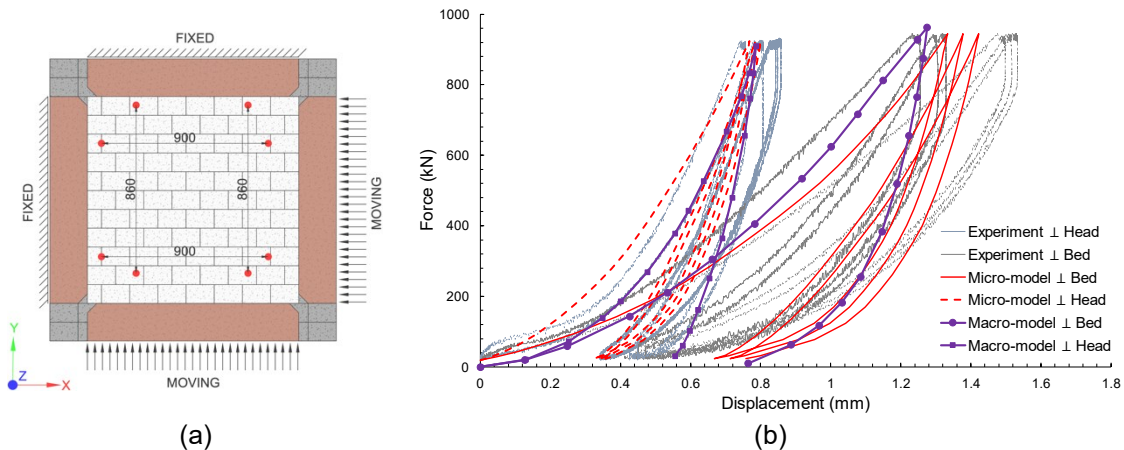


Figure 15 - Test series S08.AT.LBI – biaxial loading and unloading:
a) boundary conditions; b) experimental and numerical force-displacement diagrams.

Figure 16 makes the same observation as in Series S06.AT.LBJ and S07.AT.LHJ, where bricks are almost rigid units for a low-stress level. However, lower values of displacement can be observed in both directions as compared to the results obtained from the uniaxial tests. This global displacement reduction can be explained by the high friction forces (caused by the biaxial loading conditions) and the reduced level of stresses experienced by the masonry in these biaxial loading conditions.

Figure 17 shows the distribution of the principal compressive stress at the first peak load. From the figure, it is possible to observe the low level of stresses in the masonry units except for the areas near the support plates. This reduction in the stresses compared to the stresses observed in the previous uniaxial tests is due to the presence of biaxial loads. In this case, the force is transferred through the combination of shear and normal stresses in the masonry. The shear stresses are experienced primarily near the support and loading plates. Therefore, the masonry units undergo a low level of stress than the applied stress at the peak level. Moreover, Figure 17a presents stress distribution between different brick units in the masonry. Higher concentration of stresses can be observed between the dry joints near the boundaries. This concentration is due to friction between the ceramic plates and brick units. It can also be observed that the stresses between the joints in the central part of the wallet is lower compared to the boundary part, this is due to the transfer of forces, as explained earlier.

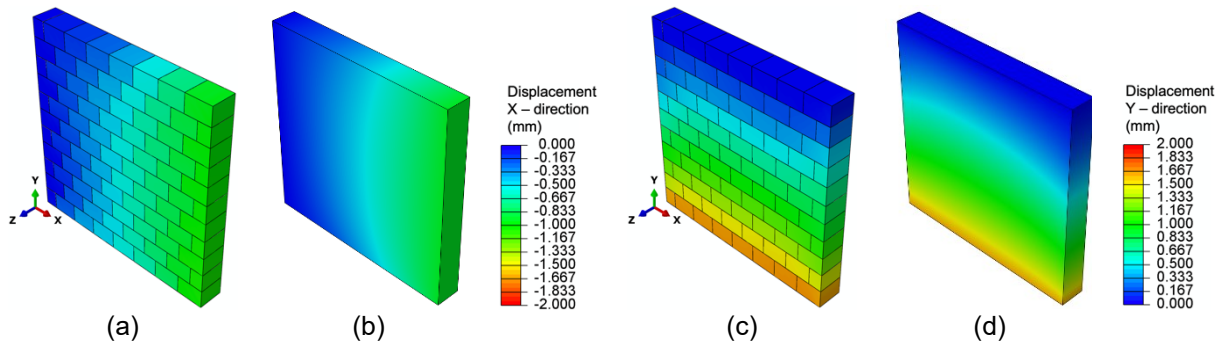


Figure 16 - Test series S08.AT.LBI - biaxial loading and unloading: Displacement along the X direction (mm) at the peak force level: a) Micro-model; b) Macro-model. Displacement along the Y direction (mm) at the peak force level: c) Micro-model; d) Macro-model.

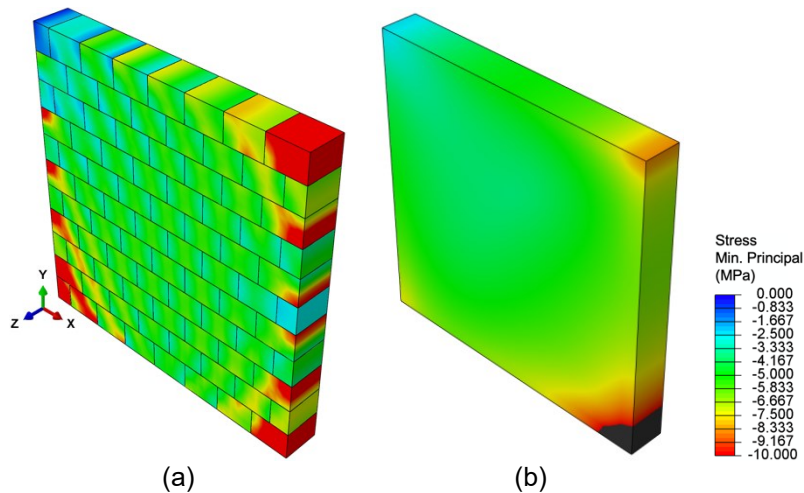


Figure 17 - Biaxial loading and unloading – minimum principal stress distribution (MPa) at the peak force level: a) Micro-model; b) Macro-model

4.5 S09.HT.CBJ: uniaxial creep behaviour - normal to bed joints

Several refractory masonry walls were tested under various thermomechanical loading conditions at high temperatures (as indicated in Table 1). These experiments aimed at evaluating the orthotropic nonlinear elastic-viscoplastic behaviour of refractory masonry at temperatures of around 1500 °C (similar to service temperatures). The solution domains used for both modelling approaches are similar to those used in the previous section (Figure 10). The temperature-dependent values of Youngs' modulus are used. More details regarding the creep parameters used and friction coefficients between the bricks at high temperatures can be found in *Deliverable D3.6*.

The FE analysis of the walls included two steps: first, transient heat transfer analysis was carried out to compute the temperature distributions and variations with time, and second, transient thermo-mechanical analysis to calculate the resulting thermomechanical stress and strain fields. In the transient heat transfer analysis, the average measured temperature variations of the cold face (CF) and hot face (HF) of the walls were applied as thermal boundary conditions. Therefore, the computed temperatures of the HF and the CF are the same as the applied temperature boundary conditions. The goal was to obtain the temperature fields through the thickness of the wall during heating, load application, holding and unloading. These, in turn, are employed as thermal loads in thermomechanical analysis. Comparisons between the experimental and numerical HF and CF temperature variations with time are given in Figure 18a. The five solid black lines represent the temperatures measured by the thermocouples in contact with the CF.

In the thermomechanical analysis, during heating, load application and load holding and unloading steps, the boundary conditions of two fixed rigid plates and the ground (top insulation layer in the test field) are set to fully fixed. During heating, the two moving rigid plates were free to move (Figure 18b). Then, during load application, load holding and unloading steps, the measured experimental reaction forces were applied as concentrated loads to the rigid moving plates.

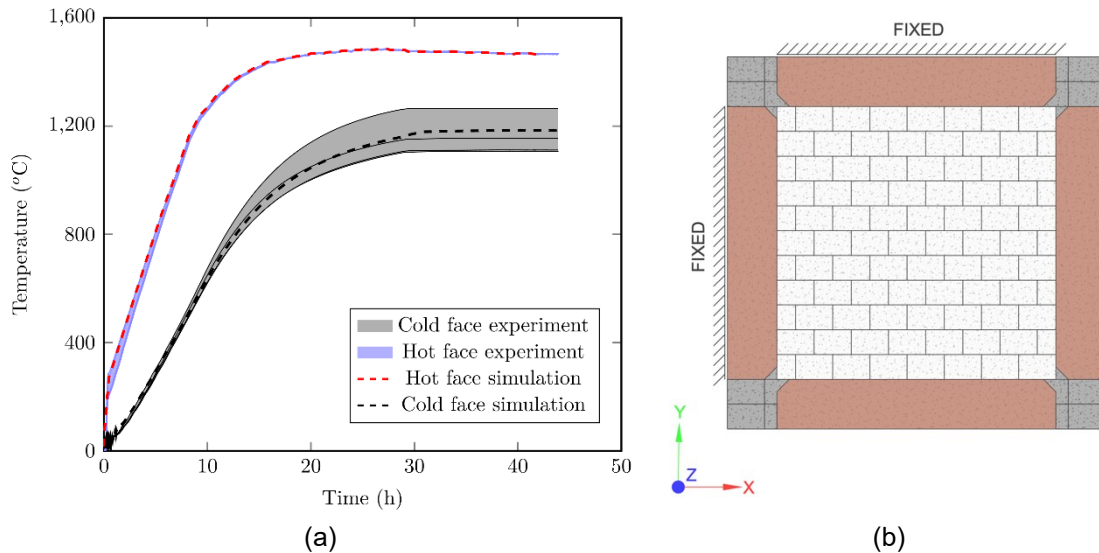


Figure 18 - Thermomechanical analysis: a) time variations of the cold and hot face temperatures during heating and mechanical testing, experimental and numerical results; b) boundary conditions for thermomechanical analysis during heating.

The obtained temperature fields of the wall and the deformed shape (for both micro and macro modelling approaches), by the end of the heating step, due to thermal expansion effects are given in Figure 19. Higher values of thermal expansion near the HF compared to the CF can be observed from the figure due to the higher temperature of the HF. As a result, the sides of the wall (in contact with the moving and fixed plungers) were not perfectly parallel to the plunger linings (wedged shape, in the depth of the wall) before the load application. The effect of thermal expansion is significant in the macro-model (Figure 19b) compared to the micro-model (Figure 19a). This difference is due to the physical presence of the dry joint in the micro-model, where the closing of the dry joints absorbs some extent of the expansion. However, a similar wedged shape can be observed in both models, resulting in higher load concentrations at the HF during the initial loading period. The thermomechanical results obtained from both models for various loading conditions are presented in the next sections.

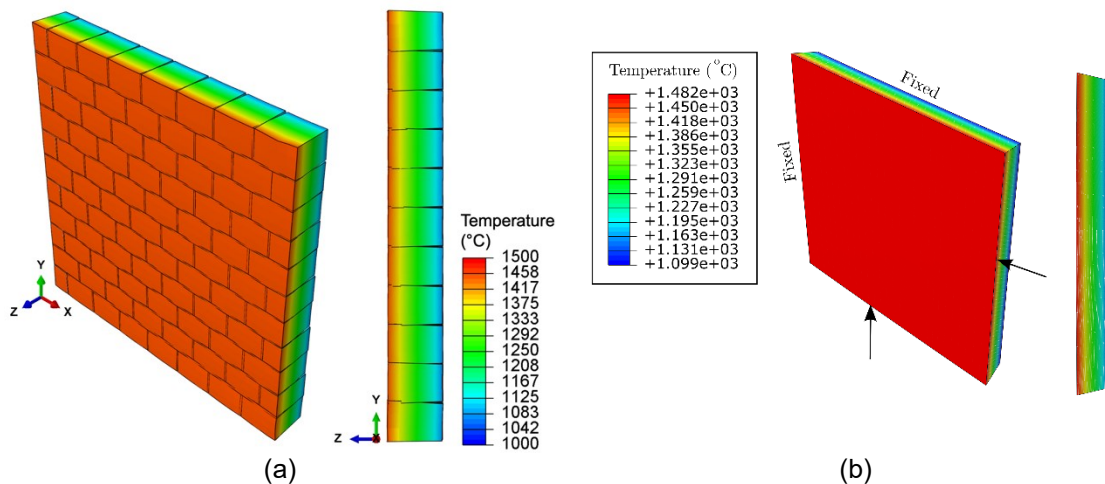


Figure 19 - Temperature distributions of the masonry wall by the end of heating step showing the deformation of the wall due to thermal expansion: a) micro-model; b) macro-model.

In test series S09.HT.CBJ, two refractory masonry walls were tested. A uniaxial compression load/unload of 4 MPa was applied in the direction normal to bed joints after the heating stage and reaching thermal equilibrium. As explained in the previous section, the two rigid plates and the ground were fixed during heating and mechanical testing. During the load application, holding and unloading steps, the experimentally measured forces were applied to the two moving rigid plates (Figure 20a).

Figure 20b presents comparisons between the experimental and numerical displacement - time diagrams during loading, holding and unloading steps. Good agreements between the numerical and the experimental results can be observed. During loading, a fast increase in the displacement can be observed due to gradual closure of joints with increasing the applied load. This increase in the displacement is higher as compared to the room temperature uniaxial compression tests in the direction normal to bed joints due to the high bulk temperature of the specimen and, therefore, lower values of Young's modulus and creep as compared

to series S06.AT.LBJ. During the holding step, an increase in the displacement of around 11 mm can be observed. This increase was mainly caused by viscoplasticity. Finally, the displacement decreased slightly during the unloading step. After load removal, the recovered displacement was very small as compared to the displacement due to the applied load. This can be attributed to the permanent deformation resulting from the viscoplastic behaviour of the structure and joints closure. The slight difference between both numerical approaches is mainly due to the creep parameters. In the micro-modelling approach, only the primary creep parameters are used, while secondary creep parameters are used for macro-model. Nevertheless, a similar behaviour can be observed from both the models, the difference in displacement during initial loading is due to different joint closure relation employed by these models.

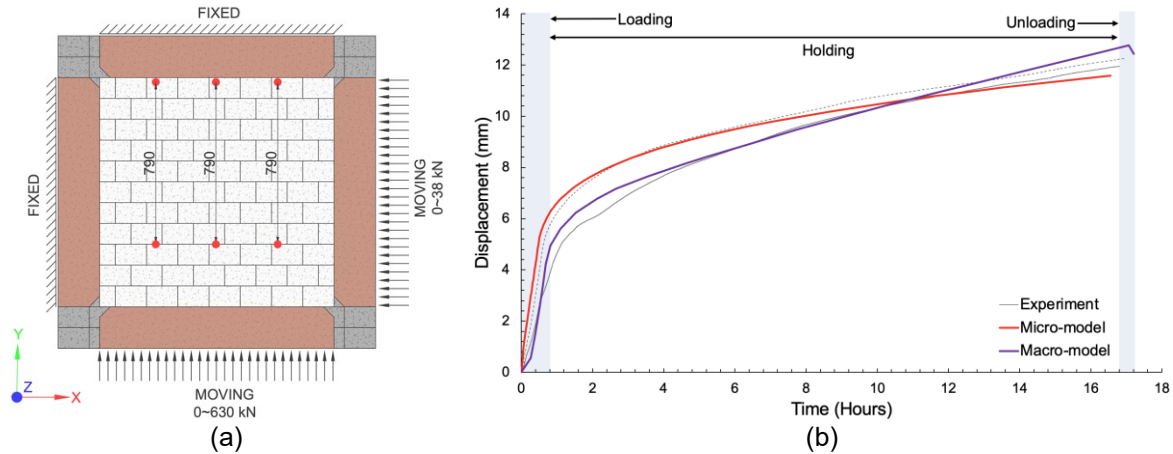


Figure 20 - Test series S09.HT.CBJ - uniaxial creep behaviour - normal to bed joints: a) boundary conditions; b) experimental and numerical time variations of the displacements during loading, holding and unloading stages.

Figure 21a and b show displacement fields in the direction normal to bed joints obtained using the micro and macro modelling approaches. From Figure 21a (micro modelling), it can be observed that at high temperatures, the bricks do not behave as rigid units as it was observed in the room temperature tests. This is due to material property degradation and creep effects at higher temperatures. The distributions of minimum principal stresses by the end of load holding step are shown in Figure 21c and d. It can be seen from the figures that the stresses observed on the HF are lower compared to those in the CF. This can be attributed to the fact that due to the lower temperature of the CF and, therefore, lower creep rates as compared to the HF, higher viscoplastic deformation rates were observed in the HF as compared to the CF. This led to a decay in the stresses in the HF due stress relaxation and an increase in the stresses in the CF during the holding step. Both models, predict a similar response for the displacement and stress distribution at higher temperatures.

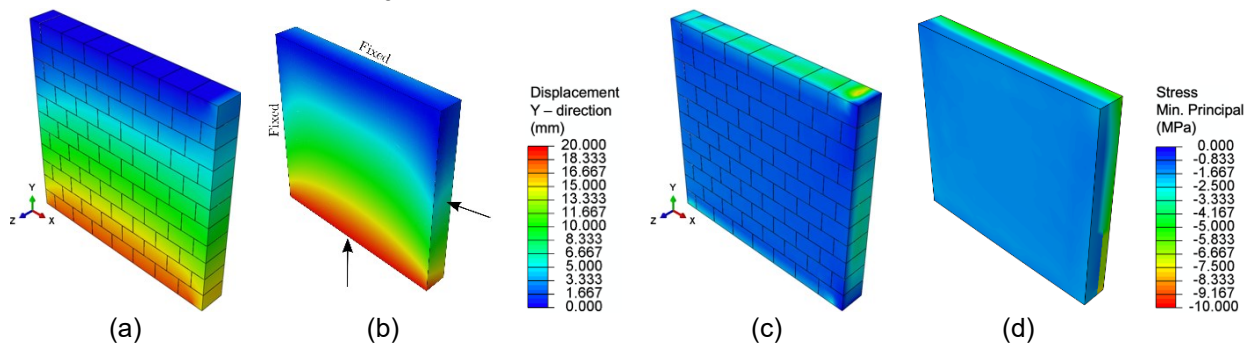


Figure 21 - Test series S09.HT.CBJ - uniaxial creep behaviour - normal to bed joints: Displacement distribution along the Y direction (mm) at 16th hour: a) micro-model; b) macro-model. Minimum principal stress distribution (MPa) at 16th hour: c) micro-model; d) macro-model.

4.6 S10.HT.CBI: biaxial creep behaviour

To evaluate the creep behaviour under biaxial loading conditions, two refractory walls were tested at high temperatures. The FE models and boundary conditions are the same as in the previous sections. After the load application step, the applied forces were held constant for 16 hours. During the load application, holding and unloading, experimentally measured forces were applied to the two moving rigid plates (Figure 22a).

Comparisons between the experimental and numerical displacement – time diagrams in the directions normal to bed and head joints during loading, holding and unloading steps are shown in Figure 22b. Good agreement between the experimental and

numerical results can be observed. The maximum displacement in the direction normal to bed joints is higher as compared to that in the direction normal to head joints due to the difference between the number of bed and head joints in the wall. However, the observed displacements are lower compared to the uniaxial creep tests performed at high temperatures. This reduction is due to biaxial force application on the refractory masonry wall which generates lower stresses in the materials and higher friction forces with the loading beams. During the holding time, the increase in the displacements in both directions were almost the same indicating full closure of bed and head joints during the loading step and therefore isotropic in-plane viscoplastic behaviour.

The displacement fields, by the end of the load holding step, in the direction normal to bed and head joints obtained using the micro and macro modelling approaches are shown in Figure 23. The minimum principal stress fields, by the end of the load holding step, in the direction normal to bed and head joints obtained using the micro and macro modelling approaches are shown in Figure 24. Displacement and stress distribution between the models are similar, however, minor differences in displacement distribution near boundaries are due to the modelling considerations. In the micro-model, a chamfered loading and support plates are considered while they are not in the macro-model.

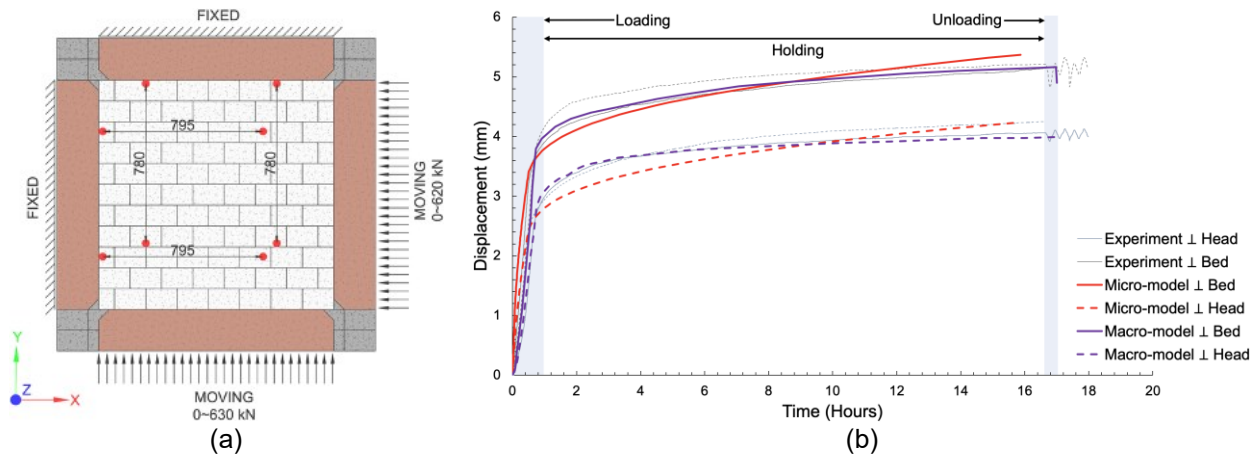


Figure 22 - Test series S10.HT.CBI - Biaxial creep behaviour: a) boundary conditions; b) experimental and numerical time variations of the displacements during loading, holding and unloading stages.

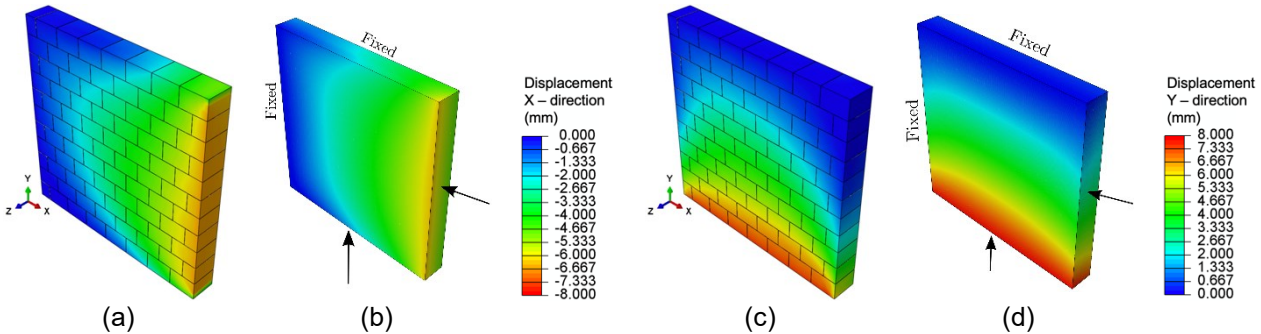


Figure 23 - Test series S10.HT.CBI - biaxial loading and unloading: Displacement along the X direction (mm): a) Micro-model; b) Macro-model. Displacement along the Y direction (mm): c) Micro-model; d) Macro-model.

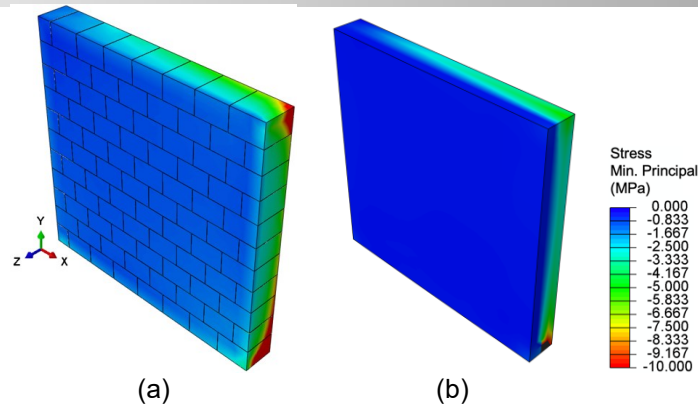


Figure 24 - Biaxial loading and unloading – minimum principal stress distribution (MPa) at the 16th hour of holding:
a) Micro-model; b) Macro-model

4.7 S11.HT.RBI: biaxial relaxation behaviour

The goal of this test series was to investigate the relaxation behaviour of the walls at high temperature. Therefore, constant strain loading conditions were employed. The modelling technique is similar to previous sections for both modelling approaches. During heating, the mechanical boundary conditions of the plungers and the ground are identical to Figure 18b. During loading, the boundary conditions are almost the same as Figure 22a with only one difference; displacement boundary conditions were applied to the moving plungers, instead of concentrated forces, and were kept constant during the holding time.

Comparisons between the experimental and numerical time variations of the resulting reaction forces, in the directions normal to bed and head joints, during two loading/unloading cycles are reported in Figure 25. Good agreements between the experimental and numerical results can be observed. During loading (1st cycle), the resulting reaction forces increased gradually to reach 600 kN. Then, when the position of the plungers was locked, a decay in the resulting reaction forces was observed due to stress relaxation caused by the viscoplastic behaviour of the structure at high temperatures. Then, the forces decreased to zero during the unloading stage. Similar behaviour was noticed for the second loading cycle. Both the models predict a similar response under this loading condition.

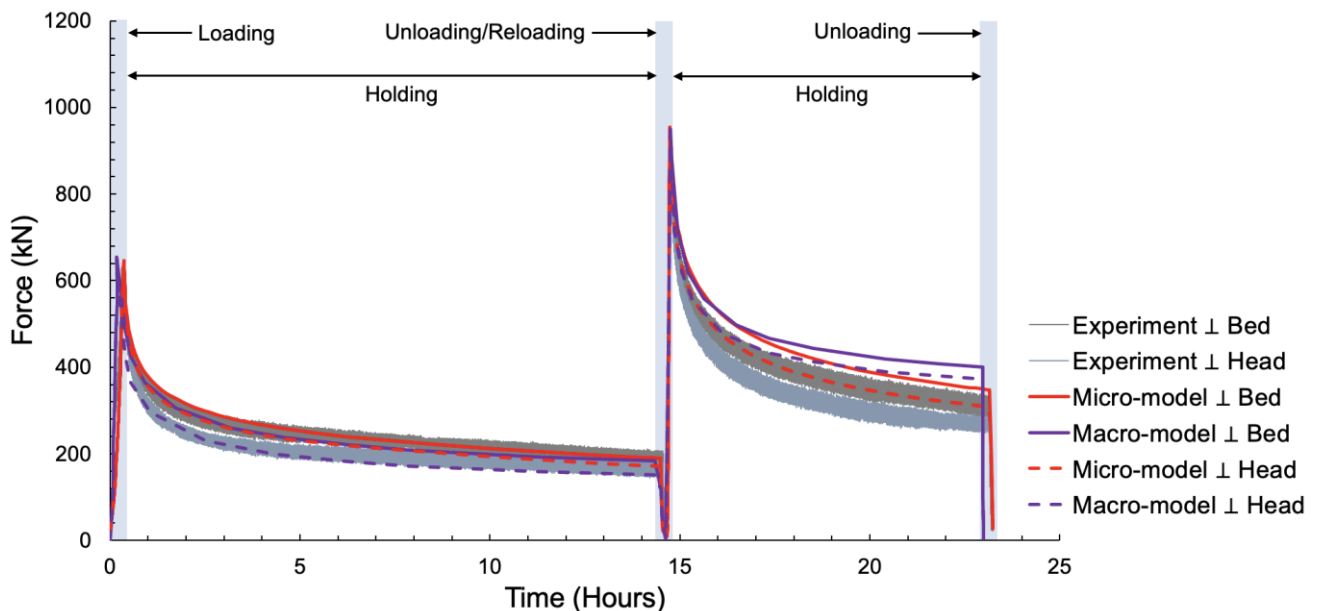


Figure 25 - Experimental and numerical time variations of reaction forces during loading, holding, and unloading stages of two testing cycles.

4.8 Comparisons of the computational time

In order to compare the computational time of both models, test series S11 has been chosen as a benchmark. The test series has been simulated using the same number of processors (8 processors). Table 2 shows a comparison between the CPU time

and wall clock time of both models. The macro model is faster than the micro model, with a length of about 10-15% of the micro model.

Table 2 - Comparisons between the CPU and wall clock time of the micro and macro models

	Micro model	Macro model
CPU time (sec)	29735	4580.1
Wall clock time (sec)	12933	1307

5 Conclusions

In this document, comparison between two modelling approaches is presented, homogenization approach (macro-modelling) and micro-modelling approach. The macro-modelling approach replaces refractory brick units and dry joints with an equivalent homogenised material. The micro-modelling approach models both the units and joints between units. The results obtained from both these approaches, show a good agreement with the experimental results.

From the results presented here, it can be observed that both modelling approaches provide a reliable prediction of masonry response at the ambient and higher temperatures, validated with the experimental results. Moreover, the response obtained by these approaches are in good agreement with each other. For the simulations, both models employ the same parameter values for the thermomechanical properties of the materials and similar boundary conditions. The primary difference between the models was the joint closure relationship. Despite this difference, the numerical responses of these models were well within the bounds of experimental results.

Therefore, both approaches can be used for the thermomechanical analyses of refractory structures. Depending on the outcome requirement, a particular approach can be selected. A homogenized model uses a simpler geometry modelling compared to micro-modelling, where all the individual units and interfaces must be modelled separately. This can be useful while modelling larger industrial structures. In general, compared to micro-models, homogenized models require less parameters to define the materials. In micro-models, additional parameters need to be defined, depending on the constitutive models used. While homogenized approach presented in this document requires formulation of various equations to identify the stiffness parameters of the homogenised elements and a user-supplied subroutine. As presented in this document, macro-modelling approach provides useful global outputs, while micro-models can provide, besides global outputs, localised output as well (for example stress and strain concentration near the joints, localised damage, and deformation). Another point to consider is the computational time. As presented earlier the computational time of the macro model is about 10-15% of the micro model, primarily due to a smaller number of interface elements to model joints. It should be highlighted that these modelling approaches can be used in combination. A global response obtained from the homogenised approach can be used to supply a localised boundary condition for a small part of a large structure to evaluate the localised behaviour of the refractory masonry.

6 References

- [1] Samadi, S., S. Jin, D. Gruber, H. Harmuth, and S. Schachner, "Statistical study of compressive creep parameters of an alumina spinel refractory," *Ceramics International*, vol. 46, no. 10, pp. 14662–14668, 2020, doi: 10.1016/j.ceramint.2020.02.267.
- [2] Vitiello, D., "Thermo-physical properties of insulating refractory materials," Ph.D thesis, Université de Limoges, 2021.
- [3] Kaczmarek, R., "Mechanical characterization of refractory materials," Ph.D thesis, Université de Limoges, 2021.
- [4] Oliveira, R. L. G., J. P. C. Rodrigues, J. M. Pereira, P. B. Lourenço, and H. Ulrich Marschall, "Normal and tangential behaviour of dry joints in refractory masonry," *Engineering Structures*, vol. 243, p. 112600, 2021, doi: 10.1016/j.engstruct.2021.112600.
- [5] Russo, S. and F. Sciarretta, "Masonry exposed to high temperatures: Mechanical behaviour and properties - An overview," *Fire Safety Journal*. 2013. doi: 10.1016/j.firesaf.2012.10.001.
- [6] Lourenço, P. B., "Computational strategies for masonry structures," PhD-Thesis, TU Delft, 1996. doi: ISBN 90-407-1221-2.
- [7] Chew Ngapeya, G. G., D. Waldmann, and F. Scholzen, "Impact of the height imperfections of masonry blocks on the load bearing capacity of dry-stack masonry walls," *Construction and Building Materials*, vol. 165, pp. 898–913, Mar. 2018, doi: 10.1016/J.CONBUILDMAT.2017.12.183.

- [8] Ali, M., T. Sayet, A. Gasser, and E. Blond, "Transient Thermo-Mechanical Analysis of Steel Ladle Refractory Linings Using Mechanical Homogenization Approach," *Ceramics 2020*, Vol. 3, Pages 171-189, vol. 3, no. 2, pp. 171–188, Apr. 2020, doi: 10.3390/ceramics3020016.
- [9] Smith, M., *ABAQUS/Standard User's Manual, Version 2019*. United States: Dassault Systèmes Simulia Corp, 2019.
- [10] DIANA FEA BV, "Diana User's Manual, Release 10.3," *DIANA FEA BV*. 2019. doi: 10.1080/15421400600788682.
- [11] International Organization for Standardization, *ISO 834-1:1999 - Fire-resistance tests — Elements of building construction — Part 1: General requirements*. Switzerland, 1999.
- [12] Oliveira, R. L. G., J. P. C. Rodrigues, J. M. Pereira, P. B. Lourenço, and H. U. Marschall, "Thermomechanical behaviour of refractory dry-stacked masonry walls under uniaxial compression," *Engineering Structures*, vol. 240, no. December 2020, 2021, doi: 10.1016/j.engstruct.2021.112361.
- [13] International Organization for Standardization, *ISO 834-1:1999 - Fire-resistance tests — Elements of building construction — Part 1: General requirements*. Switzerland, 1999.